Original Article

Ultra-Small Gold Nanoparticles with Mild Immunomodulatory Activity as a Potential Tool for Bio-Applications

(gold nanoparticles / immune cells / immunomodulation / nanoparticle-cell interaction)

T. BĚLINOVÁ[1], P. JAVOROVÁ[2], H. Y. NGUYENOVÁ[3], A. ŘEZNÍČKOVÁ[3], Z. HUMLOVÁ[2,4], M. HUBÁLEK KALBÁČOVÁ[2]

[1]Biomedical Centre, Faculty of Medicine in Pilsen, Charles University, Czech Republic
[2]Institute of Pathological Physiology, First Faculty of Medicine, Charles University, Czech Republic
[3]Department of Solid State Engineering, University of Chemistry and Technology Prague, Czech Republic
[4]Institute of Immunology and Microbiology, First Faculty of Medicine, Charles University and General University Hospital in Prague, Czech Republic

Abstract. Recently, more and more efforts are directed towards developing new imaging and drug-delivery options based on various nanoparticles, exploiting their unique properties. Here, ultra-small gold nanoparticles functionalized with widely used polyethylene glycol and its amine-terminated form were tested in respect of their potential interactions with human immune cells (cell line and primary cells). The results showed that differently terminated ultra-small gold nanoparticles represent an interesting theranostic platform as they are harmless to immune cells (not inducing cytotoxicity and severe immune response) and on the other hand, they can serve as imaging and/or drug delivery agents using e.g. monocytes/macrophages as "Trojan horses" to deliver these nanoparticles across the blood-brain barrier and diagnose or treat pathologies of the central nervous system.

Introduction

Generally, ultra-small nanoparticles (NPs) are structures with diameter up to 10 nm (Yu et al., 2016) possessing unique physico-chemical and photo-optical properties (Bera et al., 2010). Such small nanoparticles can be freely filtered by the renal system and thus be easily eliminated from circulation, representing a huge advantage for clinical application (Pombo Garcia et al., 2014). Gold-based nanoparticles are widely used in nanomedical research due to their biocompatibility confirmed by various studies (Shukla et al., 2005; Corraliza, 2014; Orlando et al., 2016).

Lately, gold-based ultra-small NPs have been mainly viewed as a potential imaging platform (Han et al., 2019), a drug carrier with the ability to invade solid tumours (Bugno et al., 2019; Luo et al., 2019), and even to enter the cell nucleus (Sokolova et al., 2020). All of these studies suggested that such NPs have high penetration potential towards both, healthy and cancerous tissue, without inducing a significant immune response. The immune system is the first line of defence of human body against foreign infections and objects. It is more than certain that this defence has developed some response mechanism to NPs (significantly dependent on the nature of NPs), which might be potentially problematic for their application in theranostics (Vivier and Malissen, 2005; Hirai et al., 2016). Thus, all novel NPs viewed as potential candidates for biomedical applications should be broadly studied in this sense.

To be able to apply gold NPs (AuNPs) in theranostics, preferably a pure and monodisperse dispersion is required. Physical methods produce very clean NPs, with the purity of produced colloids the same as the starting material (e.g., gold). On the other hand, chemical methods are very versatile in controlling NP size, shape, and thus application with the drawback of generating envi-

ronmentally unfriendly side products and limited purity of NPs (Greene, 2017). Sputter deposition of metal atoms onto liquid substrates is one of the methods producing such NPs (Wender et al., 2011). It combines the advantages of the physical vapour deposition technique and chemical colloidal synthesis (Sergievskaya et al., 2022). Polyethylene glycol (PEG) is a widely used polymeric capping agent, with neutral amphiphilic and "stealth" character for nanostructures. PEGylation of NPs (i) improves their therapeutic efficacy, (ii) prolongs circulation in blood, (iii) decreases immunogenicity, and (iv) slows down their removal by the reticuloendothelial system (Liu et al., 2015a). The hydrophilic features also improve AuNP stabilization via short-range repulsive hydration forces. Thus, PEGylated NPs do not form an extensive protein corona and should not be recognized by the immune system (Pelaz et al., 2015). Minimizing these protein-based interactions with cells (their receptors) prevents accumulation of NPs in unwanted locations, i.e., liver, spleen or bone marrow (Lu et al., 2014). Considering these outstanding properties, PEG has been approved by the Food and Drug Administration of USA for application in medicine and cosmetics (Liu et al., 2015b; Lee et al., 2021).

In this study, the interactions of ultra-small gold nanoparticles functionalized with either PEG (AuNP-PEG) or amine-terminated PEG (AuNP-PEG-NH$_2$) were studied in respect of their impact on human immune cells. THP-1 cells, as a well-established and characterized cell line, was used. These cells occur as suspension monocytes under common culture conditions; however, after stimulation with phorbol myristate acetate (PMA), they adhere and show features of macrophages. In order to mimic possible interactions of the two different AuNPs *in vivo*, peripheral-blood mononuclear cells (PBMCs) were used as an *in vitro* model system.

Material and Methods

Cells and media

Three types of cells were used in this study. The human monocytic cell line (THP-1, ATCC, Manassas, VA) was used in the monocytic form (THP-1 MONO), and after polarization with PMA to monocyte-derived macrophage-like cells (THP-1 MDMs). PBMCs from healthy volunteer donors were also used.

THP-1 MONO were seeded at a concentration of 10,000 cells/cm^2 into a sterile 96-well U-bottom plate (TPP, Trasadingen, Switzerland) in RPMI 1640 medium (Biosera, Nuaille, France) supplemented with 10 % non-heat-inactivated foetal bovine serum (FBS) (Gibco – Thermo Fisher, Waltham, MA), L-glutamine, and penicillin/streptomycin antibiotic mixture. Different concentrations of AuNP-PEG/AuNP-PEG-NH$_2$ (1, 7 and 13 μg/ml) were added and the cells were cultured in a 5 % CO$_2$ humidified controlled atmosphere at 37 °C for 24 h. For the first 6 h of incubation, the cells were kept on a shaker to increase the probability of the cell-NP interaction.

THP-1 cells were polarized into THP-1 MDMs by a 72-h treatment with 100 nM phorbol myristate acetate (PMA, Sigma-Aldrich/Merck, Darmstadt, Germany). After PMA treatment, the cells were washed and incubated for further 3 days under standard cultivation conditions. For the NP-related experiments, THP-1 MDMs were seeded at a concentration of 15,000 cells/cm^2 into a sterile 96-well flat bottom plate and pre-cultured in standard cultivation medium for 24 h. After this pre-cultivation, the cells were washed with pre-warmed PBS, and fresh cultivation medium and rising concentrations of AuNP-PEG or AuNP-PEG-NH$_2$ (1, 7 and 13 μg/ml) were added, and the cells were cultured in a 5% CO$_2$ humidified atmosphere at 37 °C for another 24 h.

PBMCs were acquired from two healthy volunteer donors by repeated blood collection (3 × 6 ml blood collected to non-coagulating tubes) along with the serum from the same volunteers (3 × 6 ml blood collected to coagulating tubes). To get the human autologous serum (HS), blood in coagulating tubes was incubated for 30 min at 37 °C, centrifuged (3,000 g, 10 min at 4 °C), and the yellow serum was aspired and stored at −80 °C until usage. To get PBMCs, the mononuclear layer of cells was separated from full venous blood by gradient centrifugation (FicollPaque, Sigma-Aldrich/Merck). After separation, the cells were seeded at a concentration of 500,000 cells/ml in 24-well plates for suspension cell culture (Sarstedt, Nümbrecht, Germany) in RPMI 1640 medium supplemented with 10% autologous non-heat-inactivated HS, L-glutamine and penicillin/streptomycin antibiotic mixture in a 5% CO$_2$ humidified atmosphere at 37 °C for 24 h. After 24 h, 13 μg/ml of AuNP-PEG or AuNP-PEG-NH$_2$ was added and the cells were cultured in a 5% CO$_2$ humidified atmosphere at 37 °C for 24 h. For the first 6 h of incubation, the cells were kept on a shaker. The blood collection from healthy volunteers was conducted under the permission of the Ethics Committee of the General University Hospital in Prague, Czech Republic and all the data are stored under GDPR.

In all NP experiments, two types of controls were conducted. Firstly, a sample of NP-untreated cells was incubated on the same plate as NP-treated samples. Secondly, to assess the influence of PEG or PEG-NH$_2$ solutions, cells treated only with the solution of corresponding PEG in dH$_2$O at the highest volume-wise concentration was created on the same plate and incubated in the same manner as the NP-treated samples.

Nanoparticles

The NPs used in this study were provided as a colloidal dispersion in dH$_2$O. The NPs were prepared by direct sputtering of gold into PEG or PEG-NH$_2$ liquid substrates and subsequently mixed with dH$_2$O (Reznickova et al., 2017, 2019). For experimental use, NPs were aseptically filtered (0.22 μm filter) and directly diluted into cell culture media.

Metabolic activity

The metabolic activity of the cells exposed to AuNP-PEG or AuNP-PEG-NH$_2$ was measured by means of an MTS assay (Cell Titer 96 Aqueous One Solution Cell Proliferation Assay, MTS, Promega, Madison, WI). The colorimetric assay determines the activity of cellular dehydrogenases. After 24 h incubation with NPs, in case of suspension cells (THP-1 MONO and PBMCs), the cell suspensions were centrifuged and the supernatants from the cells were aspired and stored for further use in −80 °C (for analysis of released cytokines). In case of adherent cells (THP-1 MDMs), supernatants were directly aspired and stored as in the previous case. To all cell types, fresh cultivation medium was added (each cell type-specific medium) and supplemented with the MTS solution at a final concentration 10 % (V/V). Cells were incubated in the incubator with a 5% CO$_2$ humidified atmosphere at 37 °C for 2 h and afterwards, their absorbance was measured (492/620 nm, Tecan Spark reader, Tecan, Männedorf, Switzerland). After the measurement of metabolic activity, the obtained values were normalized to the relative cell count acquired either by counting the cells by flow cytometry (for suspension cells, BD Biosciences FACS Canto II) or by measurement of DNA content (for adherent cells) by fluorescent staining with CyQuant NF (Invitrogen, Thermo Fisher Scientific, Waltham, MA) by a multi-detection microplate reader (Spark, Tecan).

Apoptosis/necrosis detection

Determination of apoptotic and dead cells in PBMCs after the measurement of metabolic activity was conducted using flow cytometry. The cells were centrifuged, and 300 µl of PBS containing 7-aminoactinomycin D (7AAD, BD Biosciences, Franklin Lakes, NJ) and Hoechst 33342 (Invitrogen, Thermo Fisher Scientific) was added to each well of PBMCs. The final concentration of both stains was 10 µg/ml. The cells were incubated in this solution for 30 min at room temperature in the dark. Fluorescence intensity was measured using a flow cytometer (BD Biosciences FACS Canto II). The 7AAD signal was measured with 488 nm laser and 670LP filter. The Hoechst 33342 signal was measured with 405 nm laser and emission was gained with 450/40 bandpass filter. The data were processed by FlowJo X software (BD Biosciences).

Cell surface characterization of PBMCs

Characterization of surface markers of the tested cells was conducted using flow cytometry. The THP-1 cells immediately and PBMCs after their isolation and 1 h incubation under standard conditions were washed in pre-warmed PBS and stained with antiCD11b-PE-Cy5, antiCD16-PE-Cy5 (both BD Biosciences), antiCD14-FITC, antiCD68-FITC, antiCD86-FITC (all DAKO Agilent Technologies, Santa Clara, CA) and antiCD163-BV421, antiCD206-APC (both BioLegend, San Diego, CA) for 30 min at 4 °C shielded from light. The presence of CD markers was determined in respective channels using BD FACS Canto II. The data were processed by FlowJo X software (BD Biosciences).

Cytokine release from PBMCs

Production of a wide panel of 42 cytokines was detected by the Human Cytokine Antibody Array (Abcam, Cambridge, UK). Frozen supernatants harvested from PBMCs exposed to both AuNPs were incubated with the array membrane overnight at 4 °C on a rocking shaker; all other steps were done in accordance with the manufacturer's manual. Data were processed by the ImageLab software (BioRad Laboratories, Hercules, CA). In order to achieve reference results, beside supernatants from untreated control cells (negative control), also supernatants from pro-inflammatorily stimulated cells (positive control) were used. These cells (positive control) were treated with the culture medium supplemented with 50 µg/ml of bacterial lipopolysaccharide (LPS, Sigma-Aldrich/Merck) for 24 h, on the same plate and in the same manner as AuNP-treated cells and untreated control.

Transmission electron microscopy

THP-1 MDMs were seeded at a concentration of 25,000 cells/cm^2 onto round glass slides of 15 mm diameter located in wells of a 6-well plate and incubated for 24 h in a humidified incubator at 37 °C and 5% CO$_2$ atmosphere. Then, 13 µg/ml of AuNP-PEG or AuNP-PEG-NH$_2$ was added and the cells were incubated for another 24 h. Cells were fixed in 2.5 % of glutaraldehyde in 0.1 M HEPES (Thermo Fisher Scientific) for 30 min. Then, the samples were dehydrated in a graded series of ethanol (15 min at each concentration on ice), then embedded in Quentol 651-NSA, and 80 nm ultrathin sections were prepared using ultramicrotome Leica EM UC6 (Leica Microsystems, Wetzlar, Germany) equipped with a diamond knife (Diatome, Nidau, Switzerland). The sections were mounted on formvar-coated 3.05 mm copper slots (Agar Scientific, Standsted, UK) and examined using JEOL JEM-1400 Flash TEM operated at 80 kV and equipped with a Matataki Flash sCMOS camera (JEOL, Tokyo, Japan).

Human PBMCs were incubated in RPMI medium with 10 % autologous human serum for 24 h. Afterwards, 14 µg/ml of AuNP-PEG or AuNP-PEG-NH$_2$ was added and the cells were incubated for another 24 h. The cells were attached to a cover glass covered with poly-lysine by a cytospin machine. The cells were fixed with 2 % glutaraldehyde and 2 % paraformaldehyde in 0.1 M Sörensen's sodium-potassium phosphate buffer at pH 7.2–7.4 (all Thermo Fisher Scientific). After washing, cells were dehydrated in a graded series of ethanol and embedded in LR-White resin (Sigma-Aldrich/Merck). Ultrathin sections of 80 nm were prepared using ultramicrotome Leica EM UC6 (Leica Microsystems) equipped with a diamond knife (Diatome). The sections were mounted on formvar-coated 3.05 mm copper slots (Agar Scientific) and examined in a JEOL JEM-1400 Flash

transmission electron microscope operated at 80 kV and equipped with a Matataki Flash CMOS camera (JEOL).

Statistical analysis

All the presented data (with the exception of cytokine studies) were acquired from at least three independent repetitions, each conducted at least in triplicates. Mean values are presented with standard deviations shown by error bars. Statistical analysis was conducted in the Statistica software (StatSoft, Tulsa, OK) employing non-parametric matched pair Wilcoxon test and two factor ANNOVA with post-hoc Fisher-LSD analysis. Results showing a P value < 0.05 were considered significant.

Results

Colloidal dispersions of AuNPs

Ultra-small AuNPs were prepared by sputtering gold directly into pure PEG (AuNP-PEG) or into amine-terminated PEG (AuNP-PEG-NH$_2$) (Reznickova et al., 2017). These spherical AuNPs were characterized previously and showed no toxicity for an osteoblastic cell line (Reznickova et al., 2019). Their characteristics are briefly presented in Table 1 and commented further. The average size of AuNPs determined by transmission electron microscopy (TEM) based on 300 particles was 5.9 nm and 2.9 nm for AuNP-PEG and AuNP-PEG-NH$_2$, respectively. The average size of AuNPs determined by dynamic light scattering (DLS) was 8.8 nm and 4.4 nm for AuNP-PEG and AuNP-PEG-NH$_2$, respectively. The difference in AuNP dimensions determined by TEM and DLS is caused by the fact that TEM detects only the Au core, while the DLS value includes the NP core with the PEG corona. The low merit of polydispersity index of both AuNPs shows highly uniform (monodisperse) AuNPs in colloidal dispersions (Uskokovic, 2012). Zeta potential represents the value of the surface charge of nanoparticles (Doane et al., 2012). Therefore, the negative value of zeta potential in the case of AuNP-PEG-NH$_2$ suggests that amine groups are grafted onto the surface of AuNPs and the groups with negative charge create the outer side of the NPs' corona (Kolská et al., 2014).

Cell characterization

This study is based on observation of the effect of PEGylated AuNPs on different immune cells. Firstly,

Table 1. Characterization of AuNPs by different analytical methods

		AuNP-PEG	AuNP-PEG-NH$_2$
Size (mm)	TEM	5.9 ± 0.8	2.9 ± 0.8
	DLS	8.8 ± 2.2	4.4 ± 0.9
PDI		0.201	0.252
zeta potential (mV)		−24.7 ± 4.5	−47.0 ± 1.3

the well-established and widely used THP-1 cell line was used. Under common culture conditions, this cell line is in the suspension form of monocytes (THP-1 MONO); however, after stimulation with PMA, adherent macrophages are derived from these THP-1 cells (THP-1 MDMs). Thus, this cell line was used in both forms characterized by differing morphology and surface markers (Fig. 1). It is apparent that both cell types reveal previously described characteristics (Richter et al., 2016; Baxter et al., 2020).

Since NPs used for diagnostics or treatment are administered intravenously, the first cells to encounter NPs are cells from peripheral blood. In order to mimic the *in vivo* situation, primary cells from human blood were used (PBMCs). Isolated PBMCs were characterized by flow cytometry (Fig. 2) and two types of PBMCs were detected – a small population of monocytes (about 5 %) and a larger population of lymphocytes (about 90 %). Both cell types carried specific surface CD markers. PBMCs containing both cell types in the indicated ratio were used for further experiments with AuNPs. To prevent excessive activation of PBMCs and to preserve absorption of native blood proteins, non-inactivated autologous blood serum obtained from healthy individuals was used in all cultivation experiments with their PBMCs.

Effect of AuNPs on cell behaviour

The metabolic activity of different immune cell types – suspension monocytes (THP-1 MONO), adherent macrophages (THP-1 MDMs) and suspension PBMCs – was determined after 24 h incubation with different types of AuNPs and different concentrations (Fig. 3).

AuNPs functionalized with PEG showed an interesting trend. Whereas adherent cells (THP-1 MDMs) did not respond to the presence of AuNP-PEG dramatically, suspension monocytes (THP-1 MONO) and PBMCs increased their metabolic activity in a dose-dependent manner compared to untreated control cells. As another control of the system, a volume-wise content of PEG or PEG-NH$_2$ solutions (to which the highest concentration of AuNPs was sputtered – CTRL(PEG) and CTRL (PEG-NH$_2$)) was used in the experiment to determine the reaction solely to PEG or PEG-NH$_2$.

THP-1 MONO treated with increasing concentration of AuNP-PEG dispersion increased their metabolic activity to approx. 200 % of the untreated control. However, the PEG solution without AuNPs (CTRL (PEG)) induced the metabolic rate too, but to a significantly lesser extent. An analogical effect was apparent in PBMCs, where the increase in the metabolic activity triggered by AuNP-PEG was not as high as in THP-1 MONO, while still being significant. The AuNP-PEG dispersion did not significantly change the metabolic activity of THP-1 MDMs, but the PEG solution (CTRL (PEG)) reduced their activity significantly to approx. 70 % of the untreated control, which can be evaluated as toxic.

On the other hand, the AuNP-PEG-NH$_2$ dispersion caused similar induction in the metabolic activity of THP-1 MONO and PBMCs as the AuNP-PEG dispersion.
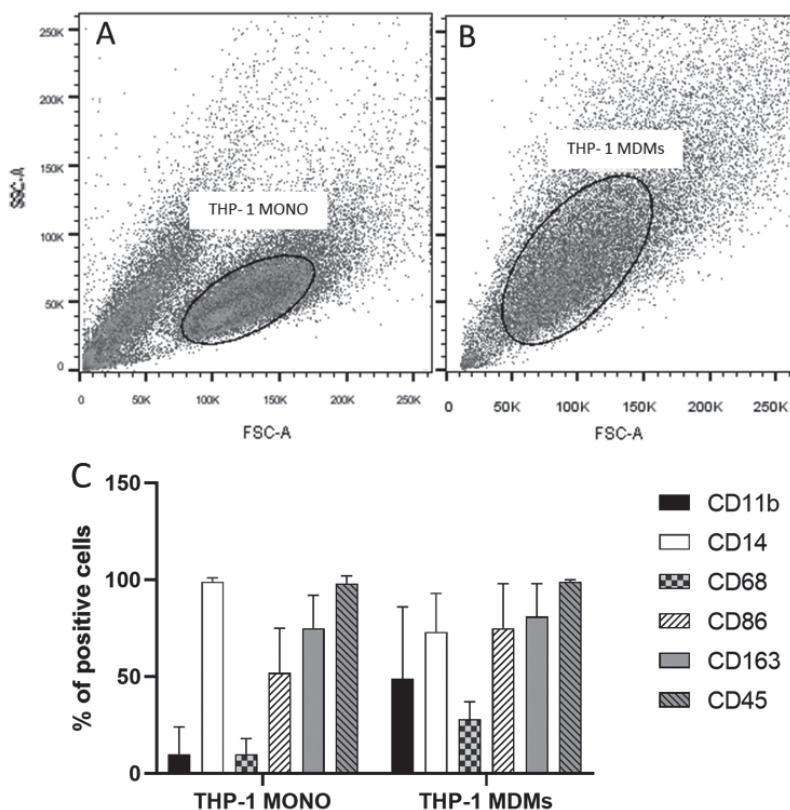
Fig. 1. Flow cytometry characterization of THP-1 cell line in the form of monocytic suspension (**A** – THP-1 MONO) and adherent macrophages after stimulation by phorbol myristate (**B** – THP-1 MDMs). Frequency of surface CD markers on these cell types (**C**).
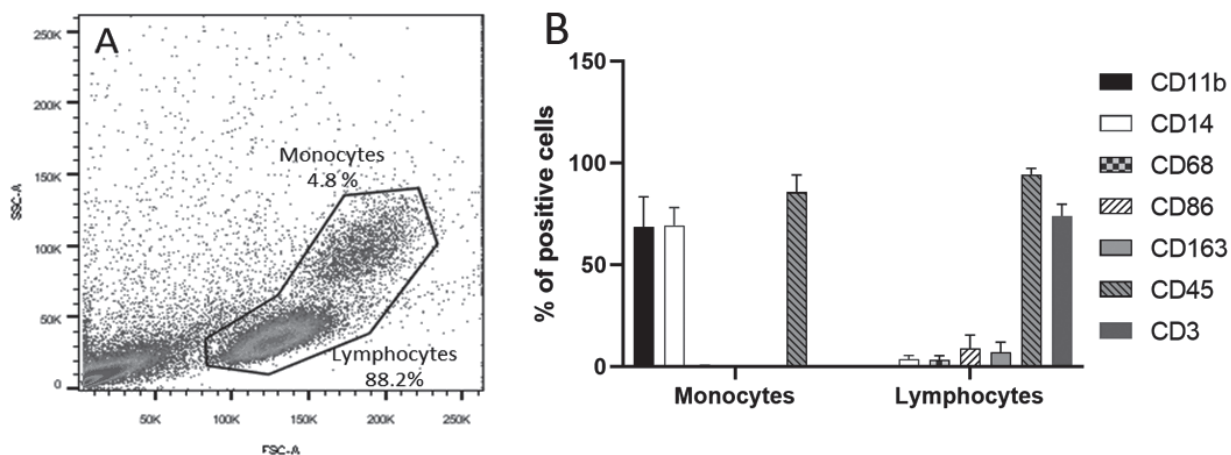

Fig. 2. Flow cytometry characterization of primary PBMCs isolated from peripheral blood of healthy human donors. Two distinct populations of cells were present – monocytes and lymphocytes (**A**). Frequency of surface CD markers on these two cell types (**B**).

However, the solution of PEG-NH$_2$ (CTRL (PEG-NH$_2$)) revealed metabolic induction identical to AuNP-PEG-NH$_2$ in these two cell types. The metabolic activity of THP-1 MDMs was slightly but significantly decreased by the highest concentration of AuNP-PEG-NH$_2$ dispersion. The PEG-NH$_2$ solution (CTRL (PEG-NH$_2$)) caused identical

reduction of THP-1 MDM metabolic activity (approx. reduction to 60 %), similarly as the PEG solution.

Additionally, the fitness of PBMCs (as the clinically relevant cell type) was assessed by determination of the level of apoptosis or necrosis induced by the tested AuNP dispersions and PEG solutions (Fig. 4). The treat-
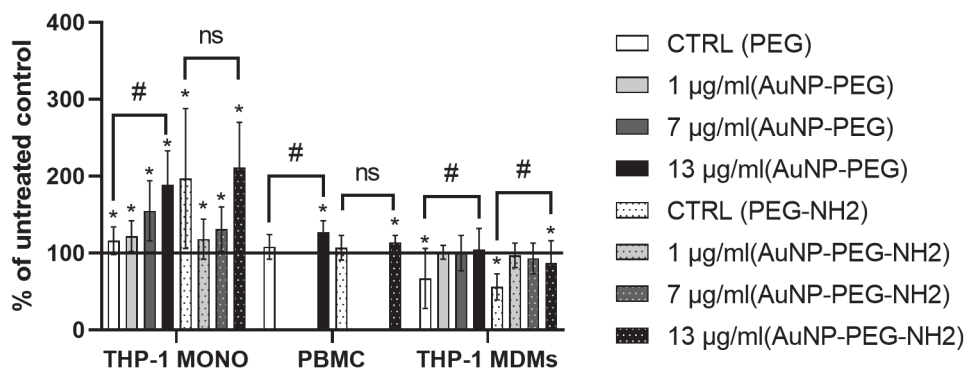
Fig. 3. Metabolic activity of immune cells – THP-1 cell line in the form of suspension monocytes (THP-1 MONO) and adherent macrophages (THP-1 MDMs) and primary PBMCs after 24 h treatment with two different AuNPs. The thick line shows 100 % of the untreated control (not shown in the column), * shows results significantly different to the untreated control (p < 0.05), # shows significant difference to a volume-wise similar content of PEG-solutions – CTRL (PEG) and CTRL (PEG-NH$_2$) (P < 0.05), ns – non-significant.
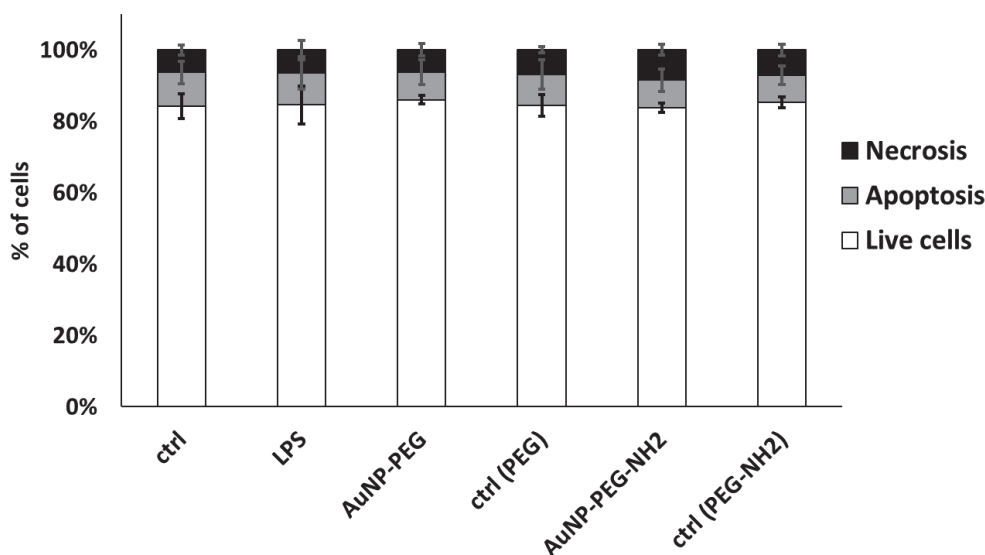

Fig. 4. Fitness of PBMCs after 24 h treatment with AuNP-PEG or AuNP-PEG-NH$_2$, bacterial LPS and PEG solutions – CTRL (PEG) and CTRL (PEG-NH$_2$).

ment did not increase the apoptotic rate or cell death significantly above a basic level of approx. 10 %, which was comparable to the untreated control PBMCs.

AuNP localization in cells

Because the tested AuNP dispersions affected the cell metabolism, it was essential to know whether AuNPs penetrated into cells. The clinically relevant PBMCs (Fig. 5), in which the AuNPs caused some metabolic effects, as well as the cell line of THP-1 MDMs (Fig. 6), in which no effect on metabolic activity was detected, were incubated with AuNP-PEG or AuNP-PEG-NH$_2$ for 24 h and analysed by TEM.

Images of the control PBMCs (AuNP-untreated) show the expected two types of cells, larger monocytes/macrophages and smaller lymphocytes (Fig. 5A–C). Orga-

nelles in the cells are not perfectly visible, because a contrast agent was not used for preparation of the samples to avoid the interference with AuNPs and their clearer visualization.

In case of PBMCs treated with AuNP-PEG (Fig. 5D–G), only a small portion of cells contained these AuNPs. The majority of the observed cells did not contain any AuNP-PEG inside them, but the AuNP-PEG were clearly present in the cell vicinity (Fig. 5D). However, some cells contained the AuNP-PEG, and in this case the AuNP-PEG formed aggregates (dense and compact, Fig. 5E) and were localized in the cytoplasm of morphologically healthy and damaged cells. Due to the used non-contrasting technique, it is hard to localize the aggregates to specific organelles, but it is obvious that they did not penetrate into the nucleus.
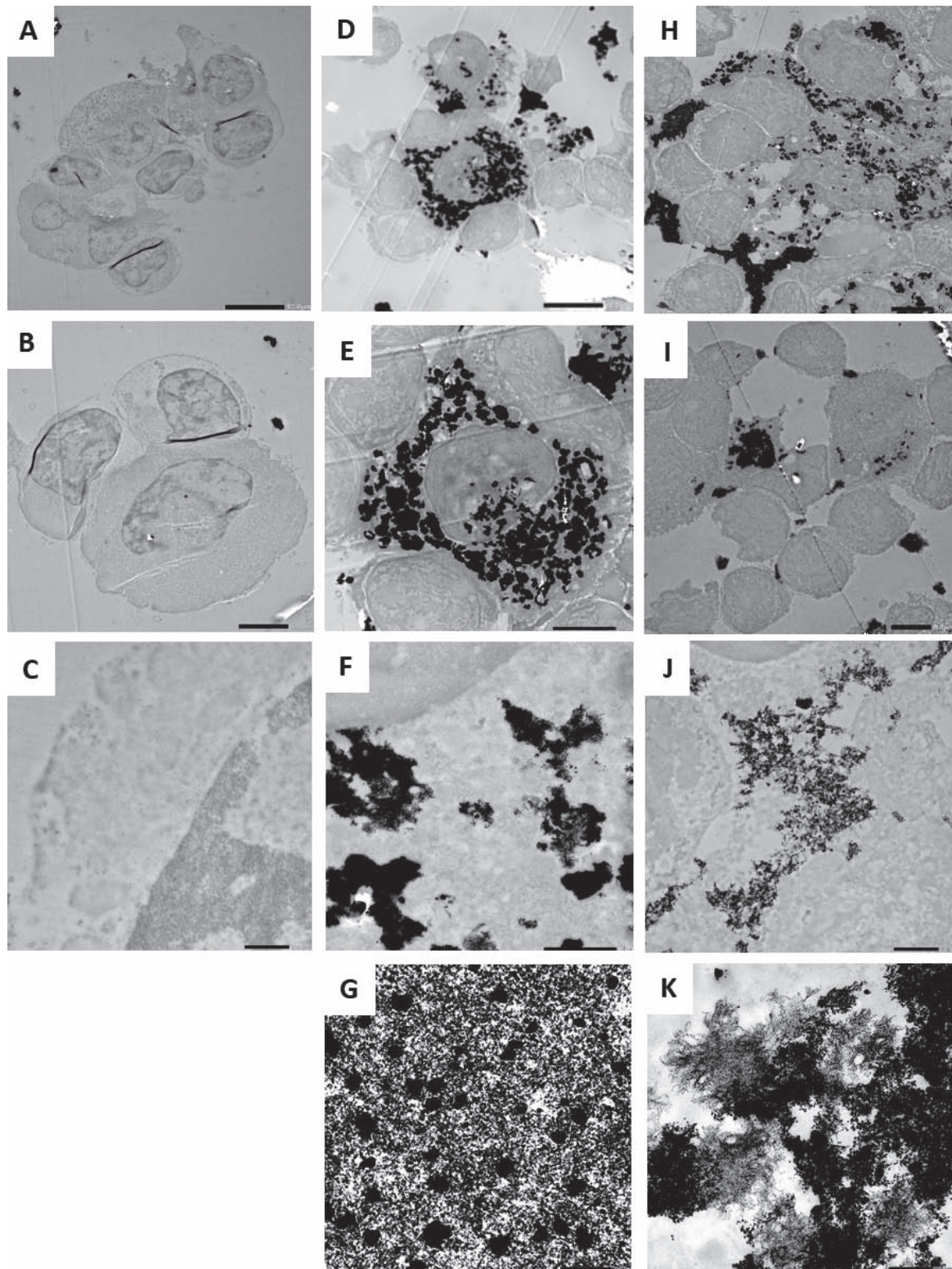
Fig. 5. Examples of TEM images of PBMCs cultivated without AuNPs (**A–C**), with AuNP-PEG (**D-G**) and AuNP-PEG-NH$_2$ (**H–K**) for 24 h. Scale bar of images – **A, D, H** = 10 μm, **B, E, I** = 5 μm, C= 0.5 μm, **F, J** = 1 μm and **G, K** = 0.2 μm.

On the other hand, AuNP-PEG-NH$_2$ were localized inside most of the PBMCs or in their close vicinity (Fig. 5H). This type of AuNPs formed two different aggregate forms (Fig. 5K). Firstly, highly dense aggregates similar to the ones observed in the AuNP-PEG-treated samples (Fig. 5F and G) formed several small clusters. Secondly, less dense aggregates were observed exclusively in this sample (Fig. 5J). AuNP-PEG-NH$_2$ often filled a large volume of the cell cytoplasm without noticeable compartmentalization.
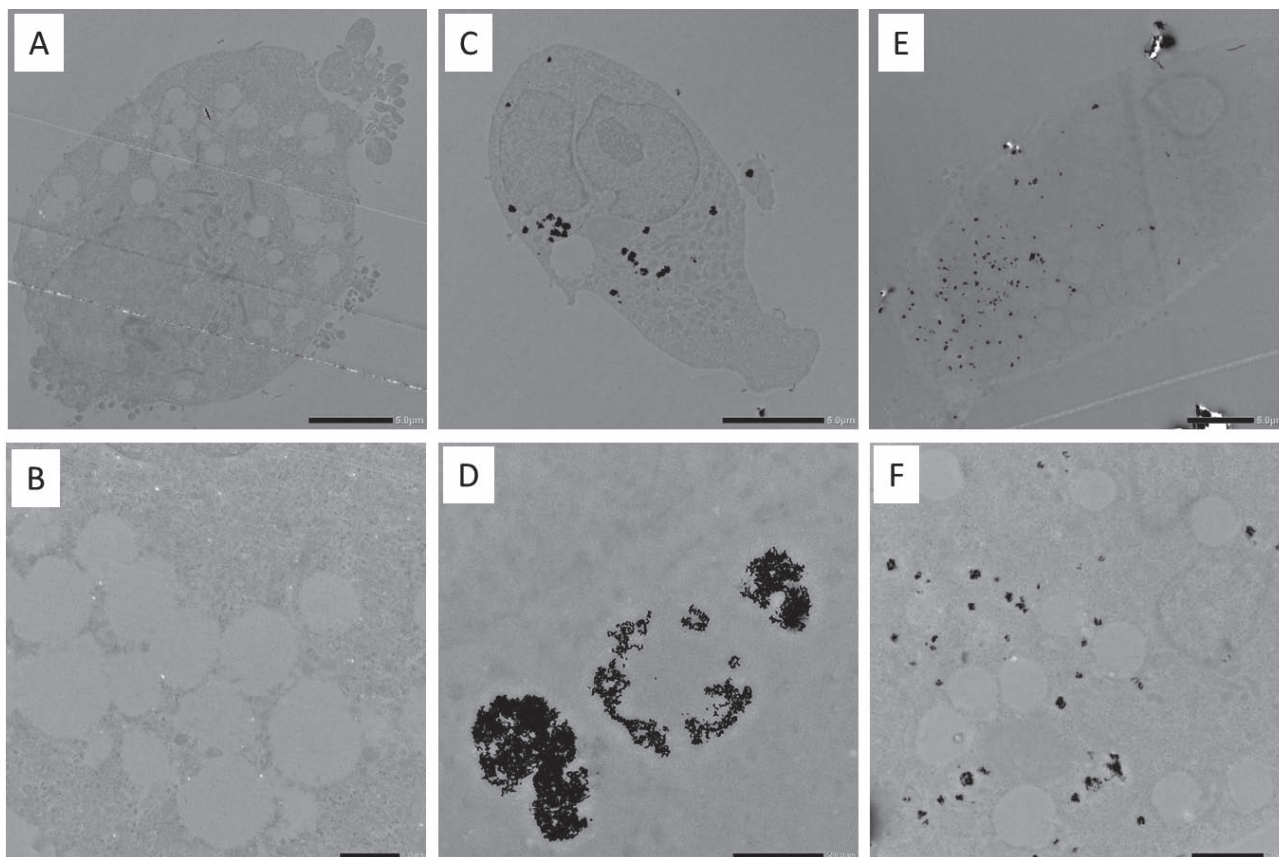
Fig. 6. Examples of TEM images of THP-1 MDMs cultivated without AuNPs (**A–B**), with AuNP-PEG (**C–D**) and AuNP-PEG-NH$_2$ (**E–F**) for 24 h. Scale bar of images – **A**, **C**, **E** = 5 µm, **B** = 1 µm, **D** = 0.5 µm and **F** = 2 µm.

Similar results were obtained in THP-1 MDMs incubated for 24 h with AuNP-PEG or AuNP-PEG-NH$_2$ (Fig. 6). Both AuNPs were localized in some vesicles inside the cells; however, their form varied. The AuNP-PEG particles formed large aggregates localized around the cell nucleus (Fig. 6C), while AuNP-PEG-NH$_2$ formed small aggregates dispersed in the cytoplasm and in some vesicles within the whole cell (Fig. 6E and F).

In conclusion, both tested AuNPs were found in PBMCs as well as in THP-1 MDMs, and their distribution pattern and characteristics were similar in respect of the individual AuNP types in both cell types.

Cytokine release after incubation of PBMCs with AuNPs

The interactions of immune cells with any nanoparticles are highly interesting especially in respect of their possible immunomodulation properties and immune system activation. In order to assess such potential of AuNPs, production of cytokines by PBMCs after incubation with AuNP-PEG or AuNP-PEG-NH$_2$ was determined. A broad panel of 42 cytokines was employed for multi-target screening and complex profile achievement (Fig. 7). Bacterial LPS was introduced as a positive inflammation control. The results showed that AuNPs interact with PBMCs and can stimulate them to release various cytokines. An enhanced release was detected for IL-1β, IL-6, GM-CSF and IL-10; however, strictly from AuNP-PEG-NH$_2$-treated cells. The AuNP-PEG dispersion induced a detectable increase in IL-6 only. On the other hand, LPS treatment resulted in a more pronounced increase in pro-inflammatory cytokines, including those detected previously as well as TNF-α. These results suggest that the intensity of AuNP-induced immune response is mild in comparison to that induced by LPS. In case of the AuNP-PEG dispersion, production of certain cytokines was even inhibited (except for IL-1β and IL-6). Data regarding the cytokines that were not detectable were omitted.

Discussion

Firstly, we characterized THP-1-MONO and THP-1 MDM cells in respect of their surface CD markers and compared them with PBMCs. The population of monocytes derived from PBMCs had the characteristics comparable to THP-1 MONO; however, some markers of polarized macrophages found in the population of THP-1 MDMs (CD11b, CD163) were also apparent. We incubated PBMCs in autologous human serum instead of FBS to create conditions as natural as possible and to try
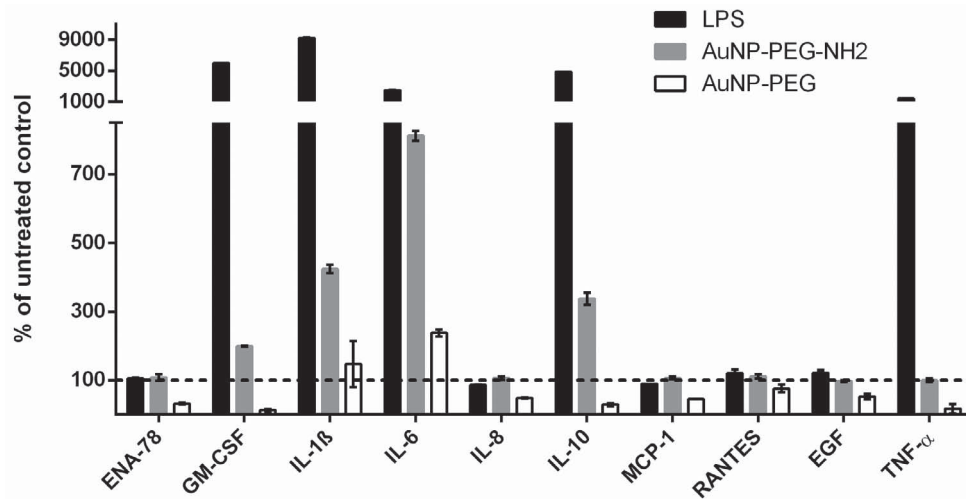
Fig. 7. Cytokine release from PBMCs after 24 h incubation with AuNPs and LPS determined by multi-cytokine panel.

to avoid polarization of PBMCs just by the xeno-derived serum components. Moreover, the use of autologous serum for experiments studying the interaction of immune cells with AuNPs is unique. We also characterized the abundant lymphocyte population derived from PBMCs, and they matched the markers of lymphocytes adequately.

Secondly, we incubated three immune cell types with AuNP-PEG and AuNP-PEG-NH$_2$ and determined their metabolic activity via detection of activity of cellular dehydrogenases. A dose-dependent induction of the metabolic activity triggered by AuNP-PEG occurred in THP-1 MONO cells and to a lower degree in PBMCs. Such stimulation effect of NPs, which under some conditions (higher dose) are cytotoxic, was already described and called hormesis (Kawata et al., 2009). The metabolic stimulation was also observed after a short-time treatment of THP-1 monocytes by ultra-small silicon-carbide NPs (Belinova et al., 2020). In longer-lasting experiments, these silicon-carbide NPs polarized monocytic cells (THP-1 MONO) to macrophage-like (THP-1 MDMs) or dendritic-like cells (Belinova et al., 2020). However, no influence on the metabolic activity of THP-1 MDMs was detected after exposure to AuNP-PEG. The PEG solution had no effect on THP-1 MONO and PBMC metabolic activity but reduced the metabolic activity of THP-1 MDMs, confirming that the effect of PEG on cells cannot be disregarded (Pham Le Khanh et al., 2022). In addition, we observed a strong effect of the PEG-NH$_2$ solution on the metabolic activity of the tested cells – strong induction in THP-1 MONO, moderate induction in PBMCs, and strong reduction in THP-1 MDMs. Thus, these reactions to the PEG-NH$_2$ solution did not allow us to attribute the apparent induction of THP-1 MONO metabolic activity by AuNP-PEG-NH$_2$ to the effect of AuNP dispersion as in the previous case, but more to the effect of the PEG-NH$_2$ solution. Despite the significant differences in the metabolic activity of

the tested cells, none of the treatments was as harmful as to cause cell death (neither apoptosis nor necrosis). Our results also suggest that the so far widely accepted inertness of PEG might not be true with the amine-terminated PEG (PEG-NH$_2$).

Thirdly, the distribution and character of AuNPs inside the tested cells differed in respect of their PEG modification. AuNP-PEG-NH$_2$, which are smaller (2.9 nm) and their zeta potential implies smaller aggregation (Shrestha et al., 2020), were found in the majority of PBMCs and in the form of less dense clusters distributed almost homogenously in their cytoplasm in comparison to AuNP-PEG. The latter AuNPs are slightly larger (5.9 nm) and their zeta potential implies higher aggregation. This is documented by just a small number of cells containing AuNP-PEG inside them, and in that case they formed large and dense aggregates. Despite different distribution and character of AuNPs within PBMCs, they induced similar effects on their metabolic activity (significant increase) but no detectable induction of cell death (neither apoptosis nor necrosis). On the other hand, the effects of the two different AuNPs on the cytokine release differed significantly (despite the fact that it was detected only semi-quantitatively). PBMCs treated with the highest tested concentration of AuNP-PEG-NH$_2$ released enhanced levels of pro-inflammatory cytokines IL-1β, IL-6, GM-CSF and IL-10, although they did not reach the level of cells treated with LPS, a broadly used inducer of the inflammatory reaction. Although a small pro-inflammatory response to these AuNPs was apparent, their harmful effect on the whole organism was not expected. Induction of pro-inflammatory cytokine release after incubation of a monocytic cell line with NH$_2$-terminated nanoparticles has been observed previously with silicon carbide NPs (Belinova et al., 2020). On the other hand, AuNP-PEG induced only IL-6 release, but the level of other pro-inflammatory cytokines found increased after AuNP-PEG-NH$_2$

treatment was below the level of the untreated control after the AuNP-PEG treatment. We can speculate that these cells react less to the AuNP-PEG, because AuNP-PEG did not enter the cells to such extent as AuNP-PEG-NH$_2$, and thus only a few cells reacted to these NPs. In the case of AuNP-PEG-NH$_2$, which were present in most of visualized cells, the immune reaction was more intense. On the other hand, the amine termination of NPs is well known as a positive stimulator of cell growth and adhesion (Faucheux et al., 2004; Hopper et al., 2014), and thus it is no surprise that PBMCs were more activated by them. While the amine termination is beneficial for cell stimulation, AuNP-PEG-NH$_2$ have high biomedical application potential – firstly to enter the cells and serve as an imaging agent, secondly to deliver a compound to cells serving as a delivery agent or to stimulate cells by inducing an immune reaction without being generally harmful.

The incubation of two different AuNPs with THP-1-MDMs (adherent differentiated cells) produced other effects. Both AuNPs were detected inside the cells in a very similar pattern as in PBMCs – dense and large clusters of AuNP-PEG localized in the vesicles, and smaller clusters of AuNP-PEG-NH$_2$ distributed homogenously in the cytoplasm. This implies that both particles enter the THP-1 MDMs cells without affecting their metabolic activity. This has already been observed with other ultra-small NPs based on silicon carbide, where SiC-NPs terminated with the NH$_2$-group had similarly no effect on the metabolic activity of macrophages but caused a significant increase of metabolism in suspension monocytes (Belinova et al., 2020). As monocytes are specialized in engulfing foreign materials inside the human body, it is anticipated that they would be prone to internalize AuNPs (with different termination) as well. Thus, these cells (monocytes/macrophages) can allow NPs to enter them without affecting their functional state.

We have shown that the ultra-small AuNPs prepared by direct sputtering into PEG or PEG-NH$_2$ solutions can be potentially viewed as a tool to be utilized in theranostics. PEGs have long been considered as biologically inert, but there is growing evidence that they are not. As much as 72 % of people have at least some antibodies against PEGs (Yang et al., 2016), presumably because of their exposure to cosmetics and various pharmaceuticals. Moreover, about 7 % of these people have the antibody level high enough to predispose them to anaphylactic reactions. Thus, the widely accepted consensus of PEG providing for a stealth effect to hide NPs from immune cells (Milla et al., 2012) should not be taken for granted and should be tested.

In this study, we demonstrated that both tested PEGylated AuNPs entered different immune cells but did not influence their activity significantly, were non-toxic and only mildly immune-stimulating. They could serve as "Trojan horses" for theranostically relevant NPs (Ali and Chen, 2015). The brain is an immunologically privileged site, which is tightly controlled by the blood brain barrier, although circulating immunocytes, such as monocytes/macrophages and a distinct subset of lymphocytes, may cross this barrier without disruption of its structural integrity (Corraliza, 2014). Thus, monocytes/macrophages appear to be the choice as cellular vehicles for the delivery of NPs to treat and diagnose CNS pathologies.

Authors' contributions

T. B. participated in data acquisition and writing and reviewing, P. J. participated in data acquisition, H. Y. N. prepared NPs, A. R. participated in writing, Z. H. provided clinical supervision over PBMC acquisition, M. H. K. provided the scientific concept, supervision and wrote, edited and reviewed the manuscript.

Institutional review board statement

PBMCs were isolated from peripheral blood of healthy volunteer donors as approved by the Ethics Committee of the General University Hospital in Prague, Czech Republic (protocol number 5/21).

Conflict of interests

The authors declare no conflict of interest.

References

Ali, I. U., Chen, X. (2015) Penetrating the blood-brain barrier: promise of novel nanoplatforms and delivery vehicles. *ACS Nano* **9**, 9470-9474.

Baxter, E. W., Graham, A. E., Re, N. A., Carr, I. M., Robinson, J. I., Mackie, S. L., Morgan, A. W. (2020) Standardized protocols for differentiation of THP-1 cells to macrophages with distinct M(IFNγ+LPS), M(IL-4) and M(IL-10) phenotypes. *J. Immunol. Methods* **478**, 112721.

Belinova, T., Machova, I., Beke, D., Fucikova, A., Gali, A., Humlova, Z., Valenta, J., Hubalek Kalbacova, M. (2020) Immunomodulatory potential of differently-terminated ultra-small silicon carbide nanoparticles. *Nanomaterials (Basel)* **10**, 573.

Bera, D., Qian, L., Tseng, T.-K., Holloway, P. H. (2010) Quantum dots and their multimodal applications: a review. *Materials (Basel)* **3**, 2260-2345.

Bugno, J., Poellmann, M. J., Sokolowski, K., Hsu, H. J., Kim, D. H., Hong, S. (2019) Tumor penetration of Sub-10 nm nanoparticles: effect of dendrimer properties on their penetration in multicellular tumor spheroids. *Nanomedicine* **21**, 102059.

Corraliza, I. (2014) Recruiting specialized macrophages across the borders to restore brain functions. *Front. Cell. Neurosci.* **8**, 262.

Doane, T. L., Chuang, C. H., Hill, R. J., Burda, C. (2012) Nanoparticle zeta-potentials. *Acc. Chem. Res.* **45**, 317-326.

Faucheux, N., Schweiss, R., Lutzow, K., Werner, C., Groth, T. (2004) Self-assembled monolayers with different terminat-

ing groups as model substrates for cell adhesion studies. *Biomaterials* **25**, 2721-2730.

Greene, J. E. (2017) Tracing the recorded history of thin-film sputter deposition: from the 1800s to 2017. *J. Vac. Sci. Technol. A* **35**.

Han, S., Bouchard, R., Sokolov, K. V. (2019) Molecular photoacoustic imaging with ultra-small gold nanoparticles. *Biomed. Opt. Express* **10**, 3472-3483.

Hirai, T., Yoshioka, Y., Izumi, N., Ichihashi, K., Handa, T., Nishijima, N., Uemura, E., Sagami, K., Takahashi, H., Yamaguchi, M., Nagano, K., Mukai, Y., Kamada, H., Tsunoda, S., Ishii, K. J., Higashisaka, K., Tsutsumi, Y. (2016) Metal nanoparticles in the presence of lipopolysaccharides trigger the onset of metal allergy in mice. *Nat. Nanotechnol.* **11**, 808-816.

Hopper, A. P., Dugan, J. M., Gill, A. A., Fox, O. J., May, P. W., Haycock, J. W., Claeyssens, F. (2014) Amine functionalized nanodiamond promotes cellular adhesion, proliferation and neurite outgrowth. *Biomed. Mater.* **9**, 045009.

Kawata, K., Osawa, M., Okabe, S. (2009) In vitro toxicity of silver nanoparticles at noncytotoxic doses to HepG2 human hepatoma cells. *Environ. Sci. Technol.* **43**, 6046-6051.

Kolská, Z., Řezníčková, A., Nagyová, M., Slepičková Kasálková, N., Sajdl, P., Slepička, P., Švorčík, V. (2014) Plasma activated polymers grafted with cysteamine improving surfaces cytocompatibility. *Polym. Degrad. Stab.* **101**, 1-9.

Lee, J. W., Choi, S. R., Heo, J. H. (2021) Simultaneous stabilization and functionalization of gold nanoparticles via biomolecule conjugation: progress and perspectives. *ACS Appl. Mater. Interfaces* **13**, 42311-42328.

Liu, H., Doane, T. L., Cheng, Y., Lu, F., Srinivasan, S., Zhu, J.-J., Burda, C. (2015a) Control of surface ligand density on PEGylated gold nanoparticles for optimized cancer cell uptake. *Part. Part. Syst. Charact.* **32**, 197-204.

Liu, G., Luo, Q., Wang, H., Zhuang, W., Wang, Y. (2015b) In situ synthesis of multidentate PEGylated chitosan modified gold nanoparticles with good stability and biocompatibility. *RSC Adv.* **5**, 70109-70116.

Lu, F., Doane, T. L., Zhu, J. J., Burda, C. (2014) A method for separating PEGylated Au nanoparticle ensembles as a function of grafting density and core size. *Chem. Commun. (Camb).* **50**, 642-644.

Luo, D., Wang, X., Zeng, S., Ramamurthy, G., Burda, C., Basilion, J. P. (2019) Targeted gold nanocluster-enhanced radiotherapy of prostate cancer. *Small* **15**, e1900968.

Milla, P., Dosio, F., Cattel, L. (2012) PEGylation of proteins and liposomes: a powerful and flexible strategy to improve the drug delivery. *Curr. Drug Metab.* **13**, 105-119.

Orlando, A., Colombo, M., Prosperi, D., Corsi, F., Panariti, A., Rivolta, I., Masserini, M., Cazzaniga, E. (2016) Evaluation of gold nanoparticles biocompatibility: a multiparametric study on cultured endothelial cells and macrophages. *J. Nanopart. Res.* **18**, 58.

Pelaz, B., del Pino, P., Maffre, P., Hartmann, R., Gallego, M., Rivera-Fernandez, S., de la Fuente, J. M., Nienhaus, G. U., Parak, W. J. (2015) Surface functionalization of nanoparticles with polyethylene glycol: effects on protein adsorption and cellular uptake. *ACS Nano* **9**, 6996-7008.

Pham Le Khanh, H., Nemes, D., Rusznyak, A., Ujhelyi, Z., Feher, P., Fenyvesi, F., Varadi, J., Vecsernyes, M., Bacskay,

I. (2022) Comparative investigation of cellular effects of polyethylene glycol (PEG) derivatives. *Polymers (Basel)* **14**, 279.

Pombo Garcia, K., Zarschler, K., Barbaro, L., Barreto, J. A., O'Malley, W., Spiccia, L., Stephan, H., Graham, B. (2014) Zwitterionic-coated "stealth" nanoparticles for biomedical applications: recent advances in countering biomolecular corona formation and uptake by the mononuclear phagocyte system. *Small* **10**, 2516-2529.

Reznickova, A., Slepicka, P., Slavikova, N., Staszek, M., Svorcik, V. (2017) Preparation, aging and temperature stability of PEGylated gold nanoparticles. *Colloids Surf. A Physicochem. Eng. Asp.* **523**, 91-97.

Reznickova, A., Slavikova, N., Kolska, Z., Kolarova, K., Belinova, T., Hubalek Kalbacova, M., Cieslar, M., Svorcik, V. (2019) PEGylated gold nanoparticles: stability, cytotoxicity and antibacterial activity. *Colloids Surf. A Physicochem. Eng. Asp.* **560**, 26-34.

Richter, E., Ventz, K., Harms, M., Mostertz, J., Hochgrafe, F. (2016) Induction of macrophage function in human THP-1 cells is associated with rewiring of MAPK signaling and activation of MAP3K7 (TAK1) protein kinase. *Front. Cell Dev. Biol.* **4**, 21.

Sergievskaya, A., Chauvin, A., Konstantinidis, S. (2022) Sputtering onto liquids: a critical review. *Beilstein J. Nanotechnol.* **13**, 10-53.

Shrestha, S., Wang, B., Dutta, P. (2020) Nanoparticle processing: understanding and controlling aggregation. *Adv. Colloid Interface Sci.* **279**, 102162.

Shukla, R., Bansal, V., Chaudhary, M., Basu, A., Bhonde, R. R., Sastry, M. (2005) Biocompatibility of gold nanoparticles and their endocytotic fate inside the cellular compartment: a microscopic overview. *Langmuir* **21**, 10644-10654.

Sokolova, V., Mekky, G., van der Meer, S. B., Seeds, M. C., Atala, A. J., Epple, M. (2020) Transport of ultrasmall gold nanoparticles (2 nm) across the blood-brain barrier in a six-cell brain spheroid model. *Sci. Rep.* **10**, 18033.

Uskokovic, V. (2012) Dynamic light scattering based microelectrophoresis: main prospects and limitations. *J. Dispers. Sci. Technol.* **33**, 1762-1786.

Vivier, E., Malissen, B. (2005) Innate and adaptive immunity: specificities and signaling hierarchies revisited. *Nat. Immunol.* **6**, 17-21.

Wender, H., Gonçalves, R. V., Feil, A. F., Migowski, P., Poletto, F. S., Pohlmann, A. R., Dupont, J., Teixeira, S. R. R. (2011) Sputtering onto liquids: from thin films to nanoparticles. *J. Phys. Chem. C Nanomater. Interfaces* **115**, 16362-16367.

Yang, Q., Jacobs, T. M., McCallen, J. D., Moore, D. T., Huckaby, J. T., Edelstein, J. N., Lai, S. K. (2016) Analysis of pre-existing IgG and IgM antibodies against polyethylene glycol (PEG) in the general population. *Anal. Chem.* **88**, 11804-11812.

Yu, M., Lei, B., Gao, C., Yan, J., Ma, P. X. (2016) Optimizing surface-engineered ultra-small gold nanoparticles for highly efficient miRNA delivery to enhance osteogenic differentiation of bone mesenchymal stromal cells. *Nano Res.* **10**, 49-63.